Numerical analysis of flexural performances of composite steel-timber beams under fire conditions

Liu, Zhiyuan; Zhang, Ben; Jia, Huijuan; Kilpatrick, Tony

Published in:
Journal of Civil Engineering and Construction

DOI:
10.32732/jcec.2023.12.3.167

Publication date:
2023

Document Version
Publisher's PDF, also known as Version of record

Journal of Civil Engineering and Construction 2023;12(3):167-185
https://doi.org/10.32732/jcec.2023.12.3.167

Numerical Analysis of Flexural Performances of Composite Steel-Timber Beams under Fire Conditions

Zhiyuan Liu[1,2], Binsheng Zhang[1,*], Huijuan Jia[2], Tony Kilpatrick[1]

1. Department of Civil Engineering and Environmental Management, School of Computing, Engineering and Built Environment, Glasgow Caledonian University, Glasgow G4 0BA, Scotland, UK
2. Department of Civil Engineering, School of Architectural Engineering, Jinling Institute of Technology, 99 Hongjing Avenue, Jiangning District, Nanjing 211169, Jiangsu, China
E-mail:Ben.Zhang@gcu.ac.uk (Corresponding author)

Received: 30 January 2023; Accepted: 30 June 2023; Available online: 10 August 2023

Abstract: Recently, a novel type of composite structure, composite steel-timber (CST) structure, has attracted much attention by combining steel and timber in an effective way to form composite structural components, which unitises the advantages of high strength and excellent ductility of steel and decent sustainability and fire resistance of timber. However, the existing research is lacking, especially in structural fire design and analysis. In this study, based on the sequentially coupled method, the commercial finite element software ABAQUS was used to numerically simulate the dynamic performances in the temperature field and the flexural behaviours in the displacement field for a typical CST beam with a steel element embedded within the Glulam and connected by adhesives and bolts under standard fire for two hours. In the numerical simulations, the temperature distributions within the CST beam were explored, and the flexural performances of the beam in the displacement field were examined. Through the comparative analysis, the temperature distributions in the embedded steel beam and the surrounding Glulam beam under one-hour standard fire verified the advantages of this type of CST beam in structural fire design. Specifically, under a 2-hour standard fire, the surrounding Glulam could still protect the embedded steel beam from sustaining too high temperatures, so as to retain most of its material properties and help maintain the bearing capacity of the whole structure and improve the refractory limit. Parametric studies on the fire resistance of the CST beam were also conducted by adjusting the bolt spacing and the protection thickness of the Glulam. The obtained results indicated that reducing the bolt spacing and the thickness of the Glulam protection layer would have an adverse effect on the temperature distributions in the embedded steel element to a large extent, and would eventually lead to its rapid heating and strength loss and the final failure of the whole CST structure.
Keywords: Composite steel-timber (CST) structure; Structural fire design and analysis; Numerical simulation and analysis; Bearing capacity; Refractory limit.

1. Introduction

In modern engineering projects, steel and timber have been widely used, especially in Europe, Canada, Japan and other countries or regions. For steel, steel has the advantages of good plasticity, high strength and good seismic performance, and steel components are easily prefabricated, transported and installed, which can greatly improve the construction efficiency and boost building industrialisation development [1]. However, its material properties are sensitive to the environmental temperatures, in particular when the temperature reaches 600°C, it will quickly lose its strength due to thermoplastics [2]. Besides, steel components have poor stability performance and are easy to lose their load-bearing capacity due to local or global buckling instabilities. As for timber, its economically curved formation, less environmental impacts, high strength-to-weight ratio and good fire resistance [3] are favoured by many architects, engineers and manufacturers. As a natural material, timber is flammable and susceptible to corrosion and moth, drying shrinkage and moisture expansions. In terms of its mechanical properties as an anisotropy material, it is fairly brittle in tension and shear but exhibits good plastic behaviours under compression and bending [4].

In order to utilise the advantages of these two different construction materials and compensate for their respective drawbacks [5], an innovative structural form, namely composite steel-timber (CST) structure, has appeared. By definition, CST structures refer to the structural systems built by combining steel and timber. Actually, the concept of compositing timber and steel involves two levels: one is the composition between the two materials at the structural member level, and the other is at the joint level. For the first level, the composite structural components can be divided into two types: the integrated structural components by combining timber

and steel together, i.e. integrated type, and the whole structure composed of basic timber or steel structural components separated from each other, i.e. separated type [6]. Based on these two forms of composition, the composite steel-timber (CST) structure has been initially developed and applied in construction engineering. Table 1 and Figure 1 illustrate some engineering examples of composite steel-timber (CST) structures around the world. It can be found that existing engineering cases focus on separated type of CST structures, while the integrated type is still rarely adopted.

Table 1. Existing engineering cases of composite steel-timber (CST) structures around the world.

No	Building Name	Location	Type
1	Kaishi's Multifunctional Recreation Hall [6]	Kaishi, Japan	Integrated
2	Richmond Olympic Oval [7]	British Columbia, Canada	Separated
3	Aira City General Sports Park Gymnasium [6]	Aira, Japan	Separated
4	Izumo Dome [8]	Izumo, Japan	Separated

(a) Richmond Olympic Oval [7] **(b)** Kaishi's Multifunctional Recreation Hall [6]

Figure 1. Illustrations of two types of CST structures with the composition at the structural member level

So far, composite steel-timber (CST) structures have been mostly investigated based on structural components, i.e. beams, columns, shear walls, flooring systems and connections rather than the overall structure. For example, Fujita and Iwata [9] conducted a series of experiments to study the flexural performances of composite steel-timber beams composed of cedar Glulam and hot rolled H steel beam sections with various joint methods and primarily explored the initial rigidities and maximum strengths of CST beams and compared with those of pure timber and steel beams. Luo et al. [10] adopted another type of beam sections with two cold-formed thin-walled steel C-sections connected by bolts and Glulam block sticks to their upper flanges and utilised finite element software ANSYS to simulate the bending test and examine its failure modes. Chiniforush et al. [11] adopted ABAQUS to develop some non-linear 1-D frame finite element models of composite steel-CLT beams, based on their previous experimental data to predict the long-term stiffnesses and load-deflection responses of CST beams under service conditions. Wang and Duan [12] studied an I-section CST column member and analysed its strains, deformations, and failure modes under eccentric loading. Hu et al. [13] proposed a novel CST column with a steel element embedded in a Glulam column, connected by adhesives, conducted axial compression tests on the specimens with distinctive lengths to identify their perspective failure modes, load-lateral deflection relationships and load-strain responses, and established a formula for determining the load-carrying capacity. Tsai and Le [14] conducted experimental investigations on the fire resistance of a new type of CST column (see Figure 2) by testing three standard sizes of specimens directly exposed to a high temperature of 700°C for 10 minutes. Liu et al. [15] carried out monotonic and low cyclic loading tests, respectively, on the composite light steel-timber shear walls and light steel keel frame specimens and examined their bearing capacities and seismic performances. Zhou et al. [16] experimentally and numerically investigated the flexural performances of two full-scale thin-walled cold-formed steel beam-OSB slab composite flooring systems with different screw spacings under monotonic static loading. Keipour et al. [17] explored the structural behaviours of CST beam-to-column connections under hogging bending moments by conducting push-down tests on eight cruciform beam-to-column connections in the laboratory. Hassanieh et al. [18] carried out a push-out test on two CST floor systems, i.e. steel-LVL and steel-CLT floor systems, connected with high-strength bolts or coach screws, and combined with the ABAQUS simulation results to verify the accuracy of the numerical method, together with further explorations on the influences of other relevant parameters.

Figure 2. Schematic diagrams of the CST column specimen under fire in the laboratory [14]

From the review above, it can be seen that there were various types of steel-timber compositions to form structural members, and main studies focused on their structural performances, especially for beam members. Generally, through the combinations of experimental investigations and numerical simulations, the maximum flexural capacities, ductility, failure modes and other aspects of these members were obtained, compared and analysed. After verifying the validity of the numerical modelling, relevant governing parameters were further studied. However, there are few researches on structural fire design and analysis of composite steel-timber (CST) members and structures.

Fire in buildings may cause enormous and even catastrophic consequences not only for the occupants of the structure, but also for society in general including consequences to people and environments as well as cultural, structural and economic losses [19]. Therefore, during structural design, fire safety has been regarded as a basic requirement for buildings that should be equally treated as the load carrying behaviour. There are two recommended methods for structural fire design and analysis to the Eurocodes, i.e. prescriptive approach and performance-based approach. The former uses nominal fires to generate thermal actions, while the latter refers to thermal actions based on physical and chemical parameters within fire safety engineering domain. In practice, the former is more commonly used. This type of approach is usually utilised based on three levels, i.e. analysis of a member, part of the structure, and the entire structure [19], and is further divided into two categories, i.e. standard fire test method and simplified calculation method. The standard fire test is based on ISO 834 and adopts the standard fire curve as the test condition to determine the fire resistance time when the structural member totally loses its bearing capacity or its fire resistance capacity. Simplification methods for steel and timber materials are different and specific methods are described in Parts 1-2 of Eurocodes 3 and 5 [20,21]. For example, in BS EN 1995-1-2 [21], two simplified calculation methods, reduced cross-section method and reduced properties method, are adopted in the structural fire design of timber components and structures.

In this research, a type of composite steel-timber (CST) beam was selected. Based on the existing research findings, the flexural performances of a standard specimen under fire conditions for two hours were explored through numerical simulations using the commercial finite element software ABAQUS, and the influences of the reduced bolt spacing and Glulam protection thickness on the ultimate bearing capacities of the composite steel-timber (CST) beam after a two-hour standard fire were investigated by adjusting the parameters based on the established numerical model.

2. Profiles of the CST, Glulam and steel beams

The CST beams for simulations in this study were assumed to be used in Canada, where the summer duration is short and the annual average temperature is relatively low. Thus, the ambient temperature could be considered to be 0°C. In addition, the composite beam could be integrated with timber or concrete floor slabs to form composite flooring systems and hence the CST beam could be seen as three sides directly exposed to fire in the structural fire analysis [22]. In order to simplify the calculations in the finite element simulations, each type of beam specimens was modelled and calculated for a 1.0 m length.

2.1 Standard CST beam

As shown in Figure 3, the standard CST beam was mainly composed of three parts: Glulam beam, steel beam and steel bolts. The Glulam beam was assumed to be formed by bonding ten Glulam blocks made of Canadian beech with epoxy ethane adhesives. The steel beam was the I-section steel beam, with dimensions of length × height × width × flange thickness × web thickness = 1000 mm × 150 mm × 100 mm × 8 mm × 6 mm, embedded in the middle of the Glulam beam with adhesives as well, and the outer edges of the steel beam flanges had a 50

mm distance to the outer edges of the Glulam beam. Standard M20 steel bolts were selected to strengthen the composition, and the steel bolts had a 200 mm spacing in the longitudinal direction and penetrated into the composite beam.

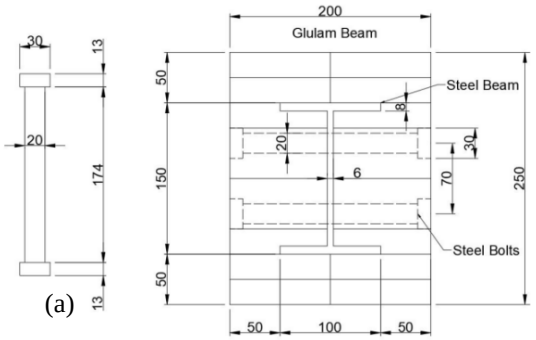

(a) (b)

(a) M20 steel bolt **(b)** Sectional view of the CST beam

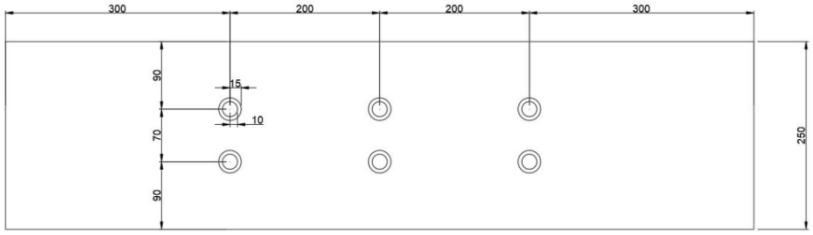

(c) Front view of the CST beam (c)

Figure 3. Profiles of the CST beam model and M20 steel bolts for the beam

2.2 Glulam and steel beams for comparison

In order to verify the advantages of this type of CST beams in terms of its fire resistance, two extra control groups were set up in this study, i.e. Glulam and steel beams with the same size as the standard CST beam. More details are shown in Table 2.

Table 2. Profiles of the CST, Glulam and steel beams for numerical simulations.

No	Type	Glulam beams (mm)	Bolt spacing (mm)	Steel beam (mm)
1	Standard CST beam	1000 × 200 × 250	200	1000 × 150 × 100 × 8 × 6
2	CST beam with reduced bolt spacing	1000 × 200 × 250	150	
3	CST beam with reduced Glulam protection thickness	1000 × 160 × 210	200	
4	Steel beam	/	/	
5	Glulam beam	1000 × 200 × 250	/	/

2.3 Standard CST beam

2.3.1 Reduced bolt spacing

Compared to the standard CST beam, the bolt spacing was reduced from 200 mm to 150 mm, which means an increase in the number of bolts per unit beam length. As shown in Figure 4, the number of bolts changed from 6 bolts in 3 rows to 10 bolts in 5 rows, but other geometric parameters of the composite beam remained unchanged.

2.3.2 Reduced Glulam protection thickness

Compared to the standard CST beam, the protection thicknesses of the outer Glulam layer for the steel beam in the height and width were reduced from the original 50 mm to 30 mm, as shown in Figure 5, giving an overall cross-section of 160 mm × 210 mm.

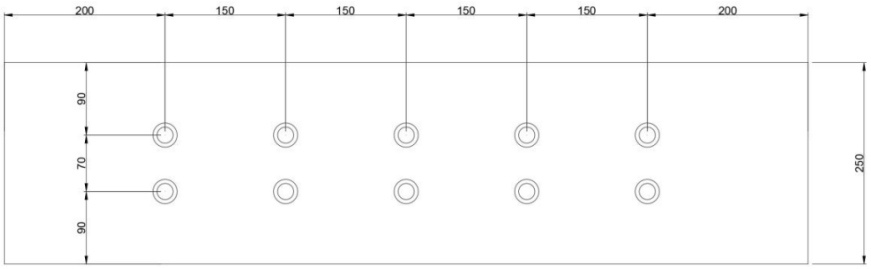

Figure 4. Schematic diagram of the CST beam with the reduced bolt spacing of 150 mm

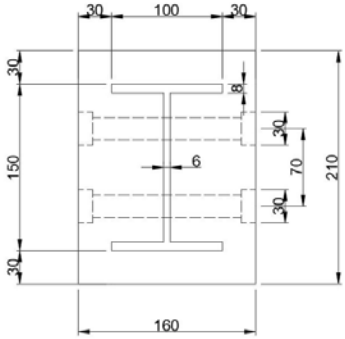

Figure 5. Section profiles of the CST beam with the reduced distance between the inner steel beam and the outer Glulam edges

3. Finite element analysis (FEA)

By considering the high requirements of laboratory equipment and the difficulty of operations, as well as the consumption of materials for subsequent parametric analyses, numerical simulations would be the most economical and efficient way. In order to accurately simulate the dynamic performances of CST beams under fire conditions, the finite element analysis technique is necessary. However, in the light of the complex geometric configurations and thermal-solid coupling analyses on this kind of CST beam model, this study adopted the finite element modelling software ABAQUS [23], as recommended in the literature. In ABAQUS, the software provides two analysis methods, the coupled temperature-displacement analysis method and the sequentially coupled analysis method [24]. The temperature-displacement analysis method is suitable for solving the problems where the temperature field and the displacement field interact together. There is indeed a significant interaction between the fields, and thus these two fields are solved simultaneously. As a result, the software has to establish matrix equations of higher-order during the calculations, which are difficult to solve and have low calculation efficiency [25]. For the sequentially coupled analysis method, the temperature field and the displacement field are independently solved according to the sequence. This method is suitable for solving the problems where there is no highly nonlinear interaction between the fields. The advantages of this type of analysis include the lower order matrix equations established by software, easy convergence of analysis results and high computational efficiency and it is adopted by many researchers. From the laboratory test results, Tsai [14] and Zhang [26] indicated that the CST specimens did not have large structural deformations and damages that affected the heat transfer and temperature field distributions in the process of fire. Some inevitable deformations were relatively small and almost had no influence on the development of heat transfer. Therefore, based on the sequentially coupled analysis method, the temperature field would be firstly operated and analysed in this study, and then the calculated results of the temperature field were imported into the displacement field as the predefined field to calculate the final bending performances of the CST beams after being exposed to fire for 2 hours.

3.1 The estimation method

The material properties, namely the thermal and mechanical properties, of steel and timber would decrease with the increasing temperature. To reduce the calculation workload of the numerical analyses and ensure the accuracy, the relationships of the material properties with the heating temperature were imported into ABAQUS based on the relevant specifications and existing research data.

For steel, its density ρ could be seen as a constant value when the surrounding temperature rises, i.e. $\rho = 7850$ kg/m^3, and the specific heat and thermal conductivity as the functions of temperature given by BS EN 1993-1-2 [20]. For timber, after fully considering water evaporation, wood carbonisation decomposition and material

composition changes during combustion, BS EN 1995-1-2 [21] presents the relationships of the density ratio, specific heat and thermal conductivity with the heating temperature.

As for the mechanical properties, steel was regarded as an isotropic material and an elastic-linear – perfectly plastic model was adopted [27]. Generally, timber materials for Glulam have different properties in normal, radial and tangential directions and can be regarded as an ideal anisotropic elastoplastic body. The cylindrical coordinate system is used to specify the material orientation in ABAQUS. All specific material characteristic data used in this study are summarised separately which can be accessed pending the request.

3.2 Setup of the numerical models in ABAQUS

During the modelling, the influence of adhesives on the temperature field was not considered. It was assumed that there was no air layer between the components. Because the thickness of the adhesives layer was small, and the heat from the external fire site would be quickly transferred to the interior components. All parts in the specimen model adopted 3D deformable solid base type, and the auto-mesh method (3 mm fine mesh around the bolt holes and 15 mm loose mesh for other areas) was applied according to the configuration characteristics of the parts. The final assembled model is shown in Figure 6.

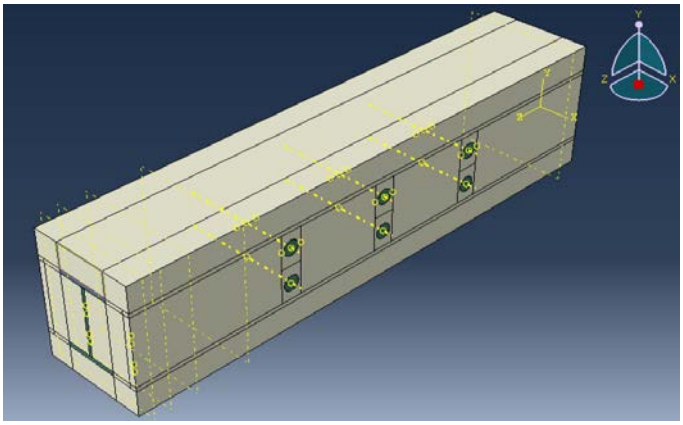

Figure 6. The final assembled CST beam model in ABAQUS.

For the step definition, heat transfer should be selected as the step type, transient analysis as the response type, and the time period should be set as 7200 seconds equal to the combustion test duration. The "Static, General" type of step with one second time period should be set for the displacement field. Besides, external fire site should be applied in the temperature field by defining an amplitude based on the standard fire curve, while in the displacement, the uniformly distributed load should also be directly applied on the top of the composite beam in the pressure form of 100 kN/m^2. As to the boundary conditions, the absolute zero temperature, the Steve-Boltzmann constant (5.678×10^{-8} W/m^2K^4) and the ambient temperature, the emissivity values (0.7 and 0.8 for steel and timber) and convection coefficient (25 $W/m^2°C$) [27] should be defined in advance to facilitate the calculations and analyses of heat conduction, radiation and convection in the temperature field. As to contact definitions, in the normal direction, hard contact was defined to apply no restrictions to the pressures transferred between the timber and steel and the Coulomb's friction model [26] with the friction coefficients of 0.3 and 0.001 for steel-timber and steel-steel contacts. During the flexural performance analysis, both ends of the composite beam in two directions shall be restricted, for the simulation requirement of a simply supported beam. More modelling details can be found from the ABAQUS User Manual [24].

4. Numerical simulation results and analysis

As discussed above, for the sequentially coupled method, the temperature field and the displacement field were calculated separately. The temperature field was calculated first, and then the node temperature results were conveyed to the displacement field model for the flexural performance analysis.

4.1 Simulation results and analysis of the temperature field

4.1.1 Temperature distributions

1) Glulam

As shown in Figure 7(a), since the CST beam was assumed to be exposed to fire on three sides, and the Glulam, serving as the protection layer, firstly sustained heat transfer between itself and the surrounding fire environment.

Therefore, the calculated node temperature of the outermost layer of the Glulam quickly reached a high value, up to 1000°C, while the top surface of the Glulam beam was not directly affected because it was embedded within the floor slab, and the surrounding temperatures there were relatively low, ranging from 100°C to 300°C. In addition, the overall temperature distribution presented a trend that node temperature would decline from the outside towards the centre, where it had the lowest temperature, which is consistent with the test results in the literature [26].

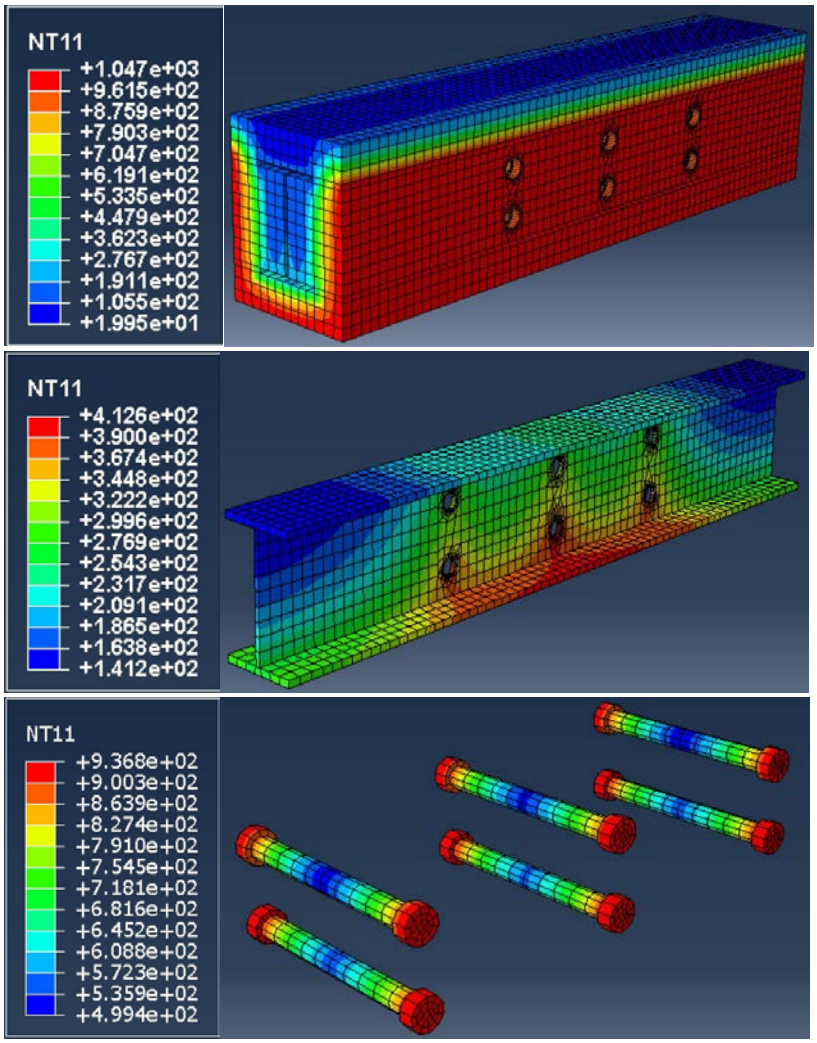

(a) Glulam beam

(b) Steel beam

(c) Steel bolts

Figure 7. Node temperature contours of the Glulam beam, steel beam and bolts at t = 120 min

2) Steel Beam

From Figure 7(b), it is clear that the web and lower flange of the steel beam were the parts with the highest temperatures of the whole beam, namely 350°C ~ 420°C. Because in the middle of the web, there were some bolt holes, where steel bolts were through the beam, and the heat carried out by the steel bolts was transferred to the interior of the CST beam. This led to rises in the node temperatures near the bolt holes of the steel webs, especially around the bolt holes near the bottom surface of the CST beam, which bear the double heat penetration from all three heat transfer directions of the fire field and from the external bolts, so the temperatures became the highest. The upper flanges at both ends of the steel beam were far away from the thermal penetration of the bolt holes and were insulated by the outer Glulam beam. Therefore, the node temperature did not increase significantly and remained at approximately 150°C.

3) Steel Bolts

As shown in Figure 7(c), when setting up the display group, the six bolts were chosen together to facilitate the comparative analysis. As a whole, all 6 bolts showed the characteristics of high temperatures at both ends and lower temperatures in the middle. The reason for this was that both heads and nuts of the bolts were exposed first to fire conditions, and were surrounded by the Glulam beam, so the heat would mainly extend along the bolt direction, which was in line with the engineering practice. Furthermore, the temperature distributions of the lower

bolts were slightly different from the upper ones and more unfavourable, which were consistent with the differences in the temperature distributions of the bolt hole areas adjacent to the lower and upper flanges of the steel beam, due to the uneven heat transfer from the fire field on three sides of the CST beam. However, the temperatures of the central bolts at the mid-span were higher than those of the bolts near the supports, which may be due to the superposition effect of the temperature penetrations from the bolts on the left and right sides.

4.1.2 Assessment of the protection ability of the Glulam

In this subsection, through the analysis of the temperature field distributions for four critical time durations, the temperature field variations of the steel beam during the whole fire process were analysed, the protection effect of the outer Glulam on the steel beam was evaluated, and the possible subsequent impacts on the displacement field were discussed.

1) Stage One

The CST beam model had been subjected to the external fire for 15 minutes (see Figures 8(a) and 9(a)). At this stage, according to the standard fire curve, the ambient temperature completed nearly 70% of the final temperature loading, i.e. 738.6°C, and the temperatures around the heads and nuts of the steel bolts reached approximately 260°C. However, the overall temperature of the steel beam was no higher than 30°C because the outer Glulam beam provided good insulation, which was highly consistent with the Tsai's test results [14], and the protection effect of the outer Glulam was reliable and effective within the first 15 minutes under the fire conditions. In addition, due to the heat conduction of the bolts through the CST beam, the temperature growth of the steel beam started from the bolt holes in the steel web and gradually extended to the flanges and both ends of the steel beam.

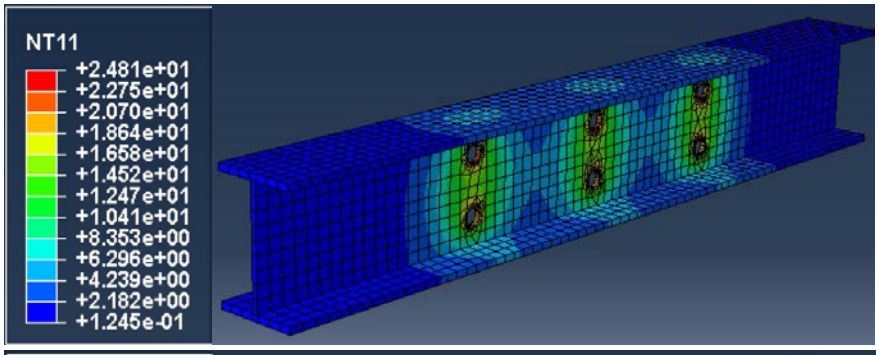

(a) t = 15 min

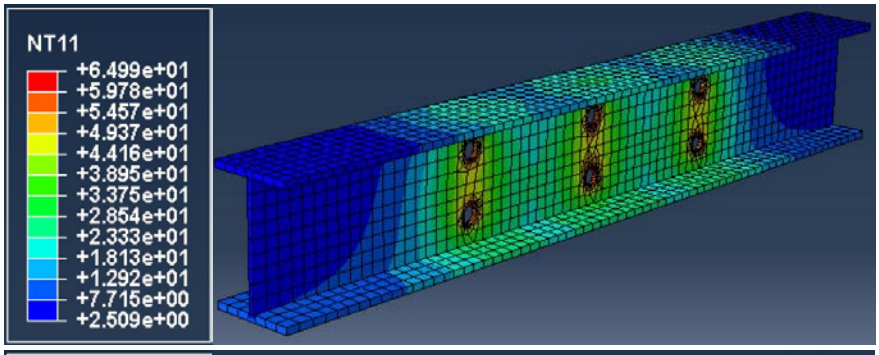

(b) t = 30 min

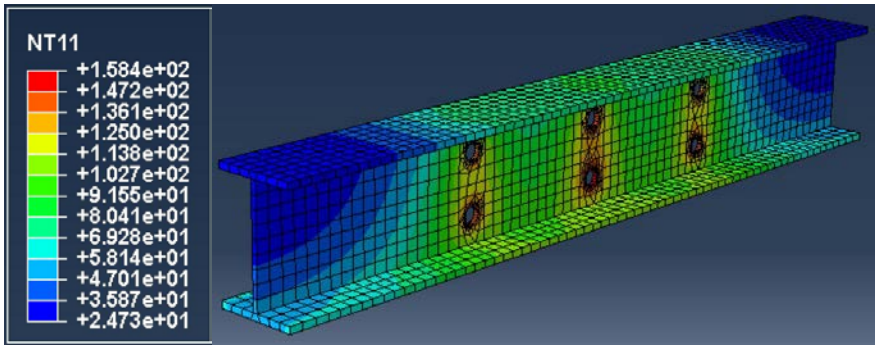

(c) t = 60 min

Figure 8. Node temperature contours of the steel beam at t = 15 min, 30 min and 60 min

2) Stage Two

When the whole structure was exposed to fire for 30 minutes, the external ambient temperature reached 841.8°C. The temperature distributions in the steel beam showed the higher temperatures in the areas of the bolt holes at the mid-span, around 50°C ~ 60°C, and lower temperature at both ends. Through the influence of heat penetration from the steel bolts, the outer Glulam still effectively prevented the heat transfer of the external fire field in the first 30 minutes, and well protected the steel beam from excessive temperature rise. However, it can be seen from Figure 8(b) that, compared with the temperature field distributions in the first 15 minutes, the temperature "diffusion" effect in the middle of the steel beam was intensified over time, the affected zone began to expand, and the effect was superimposed in the areas of the bolt holes at the mid-span. This kind of superimposition effect could also be seen on the 6 steel bolts as shown in Figure 9(b) and the middle two bolts presented relatively poor temperature distributions.

3) Stage Three

When the standard fire curve was applied for 60 minutes, the ambient temperature gradually increased to 945.3°C. At this point, the temperature field near the areas of the bolt holes in the middle of the steel beam was significantly superposed, and the temperatures in the area at the mid-span were the highest, which was presented by the software with the large red block (see Figure 8(c)). In addition, the mid-span temperature "diffusion" increased further and extended to the lower flanges at both ends of the beam, but the temperatures in the upper flanges at both ends remained below 50°C. Combined with the temperature field distributions of the bolts at this time (see Figure 9(c)), the node temperatures in the middle of the bolts had reached the temperature range of 330°C ~ 400°C, while the maximum temperature in the middle of the steel beam was only about 160°C, presenting a "gap" of heat transfer. This may be because when the bolts temperature rose rapidly, part of the heat was absorbed by the surrounding Glulam beam, while the rest was absorbed by the steel beam. In other words, the internal Glulam played a vital role in absorbing and blocking the fire heat transferred from the bolts.

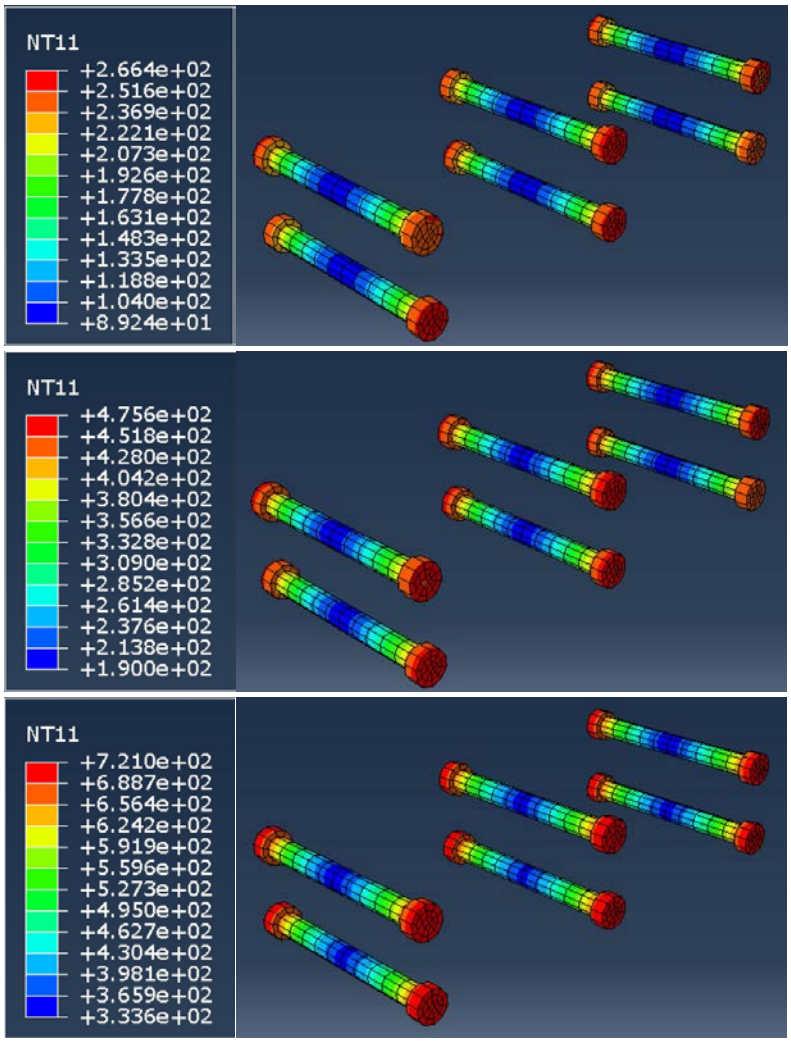

(a) t = 15 min

(b) t = 30 min

(c) t = 60 min

Figure 9. Node temperature contours of the steel bolts at t = 15 min, 30 min and 60 min

4) Stage Four

At this time, the temperature increment of the external fire site levelled off and reached 1049°C, and the temperature load acted for quite a long time. However, from Figure 7, the highest temperature zone of the steel beam occurred in the web and lower flange of the mid-span, reaching about 410°C, while most areas were in the range of 200°C ~ 300°C. This distribution characteristic was similar to that at the 60-minute stage where the temperatures at both ends were low and the temperatures near the mid-span were high. According to the typical stress-strain curves of the steel at elevated temperatures, the mid-span of the inner steel beam could retain most of its yield strength, and more strains could be spared for deformations, showing stronger plasticity even at the 120-minute fire stage.

Figure 10 shows typical stress-strain curves of steel [29] and the corresponding reduction factors for the yield strength and elastic modulus at elevated temperatures [20]. From Figure 10, the values for some thermal parameters are acquired.

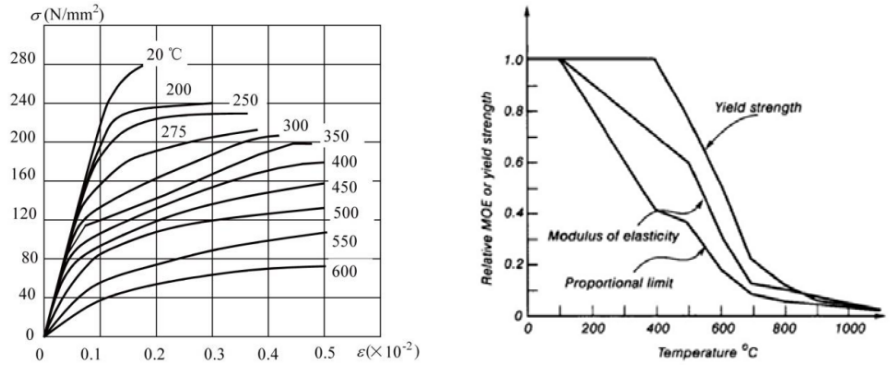

Figure 10. Typical stress-strain curves of steel [29] and its corresponding reduction factors of the yield strength and elastic modulus at elevated temperatures [20]

4.1.3 Analysis of the charring results of the Glulam beam

For the ABAQUS simulations, the timber elements with temperatures exceeding 300°C could be regarded as the carbonised layers. Charring rate refers to the ratio of the depth of the charring layer to the fire exposure time, which is also an important index to verify the accuracy of the heat transfer model. The charring rate is not constant [26], and the formation of the charring layer hinders the heat transfer to the interior. Therefore, with the increase of the heating time, the charring rate decreases.

The charring depths and charring rates were roughly calculated (based on the bottom surface) by analysing the temperature field distributions of the CST beam section in four time durations (see Table 3). According to the calculated data in the table, it can be found that the charring depth increased with the increase of the acting duration of the standard fire curve, while the charring rate decreased as the process continued, which would basically conform to the law mentioned above. Besides, with the increase of the charring depth, the outer Glulam gradually lost its ability to protect the steel, and Figure 11(b) shows that a 50 mm outer Glulam protection layer for the steel beam was basically burned out completely. If the fire temperature kept rising, the temperatures in the steel beam would quickly increase, eventually causing the complete strength loss of the steel.

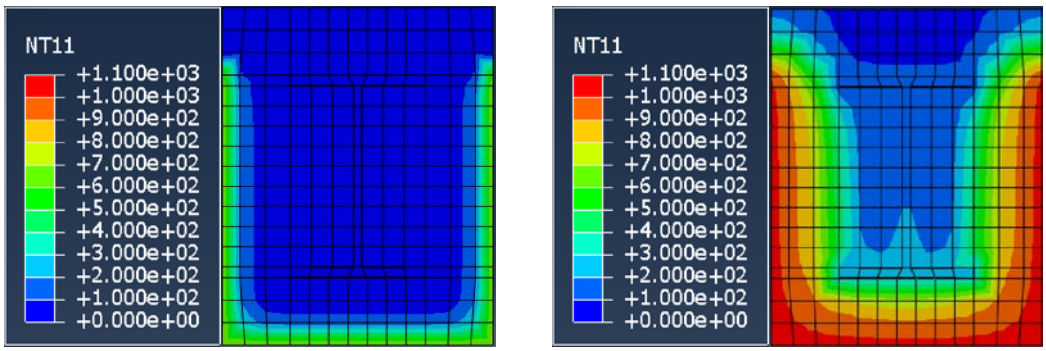

(a) t = 15 min **(b)** t = 120 min

Figure 11. Temperature field distributions of the CST beam section at t = 15 and t = 120 min

Table 3. Profiles of the CST, Glulam and steel beams for the numerical simulations.

Time duration (min)	Charring depth (mm)	Charring rate (mm/min)
15	13.3	0.89
30	20.2	0.67
60	30.1	0.50
120	49.8	0.42

4.2 Simulation results and the displacement field

4.2.1 Analysis of the simulation results

1) Displacement of the steel beam

Figure 12(a) illustrates the 3D displacement contour of the embedded steel beam. It can be seen that the maximum displacement appeared in the mid-span region and decreased from that region toward both ends. This was consistent with the displacement distribution of a simply supported steel beam under bending actions at room temperature. Under the uniformly distributed load of 100 kN/m^2 (i.e. 10 kN/m line load), the maximum displacement was 9.65 × 10^{-5} m, or 0.0965 mm. According to the linear relationship between the maximum mid-span displacement and bending loads applied on the steel beam, combined with the generally recognised deflection limit of L/360 under service loading, the maximum load capacity could be estimated to be close to 300 kN/m, which was also consistent with the engineering practice. Therefore, this served as an initial validation for the established model and based on this, reflected a good stiffness or deformation capacity for the embedded steel beam maintained within the 2-hour fire conditions.

2) Stress

Figure 12(b) illustrates the 3D von Mises stress contour of the steel beam embedded in the Glulam beam. It can be seen that the lower flange of two ends and the upper flange in the middle span region of the steel beam sustained unfavourable stress distributions. This may be because the steel beam at this moment had a tendency of buckling on both sides of the upper flange under the applied uniformly distributed load, and the lower flange in the middle span, subjected to the highest bending moment, was weakened by the bolt holes in the web, resulting in strong stress concentrations. The general trends matched the original expectations and were similar to the generally recognised stress distributions of the steel beam under the bending action. However, due to the restrictions of the outer residual timber beam, the stress distributions of the embedded steel beam were not very obvious.

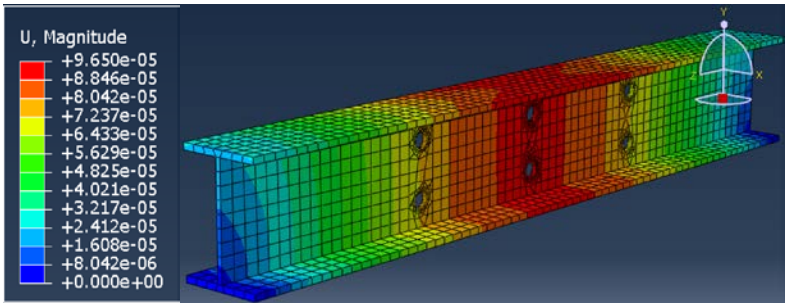

(a) 3D displacement contour (m)

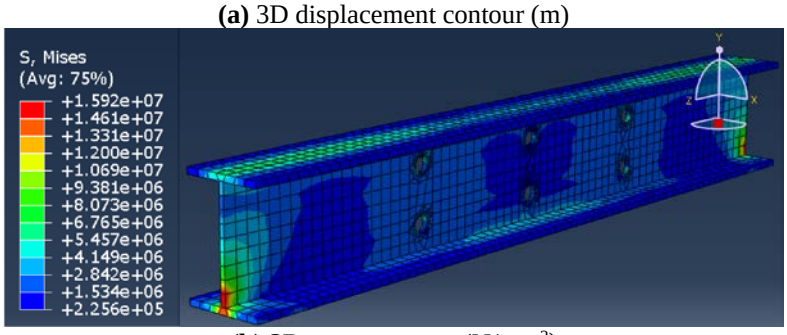

(b) 3D stress contour (N/mm^2)

Figure 12. Simulated output results of the embedded steel beam in the displacement field

4.2.2 Manual estimation calculations

In order to explore the load-bearing capacity of the CST beam, the maximum bending moment and the corresponding deflection of the simply supported steel beam embedded in the Glulam beam under the UDL applied on its upper flange were calculated according to the numerical results on the temperatures of the steel beam obtained in the temperature field and using the reduced material properties. First of all, Figure 13 illustrates the simplified calculation diagram of the steel beam and the geometrical parameters of its cross-section by ignoring the imperfection effect caused by the bolt holes in the steel web. It was also assumed that the value of UDL acting on the steel beam was w in kN/m, including the self-weight of the steel beam and the variable loads on the upper flange.

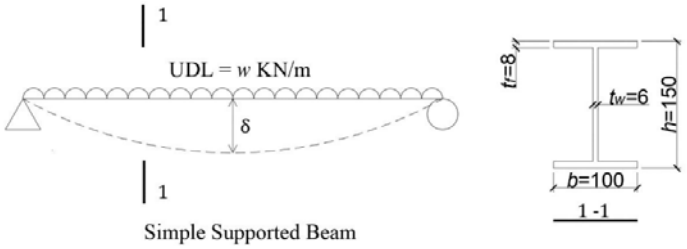

Figure 13. Illustration of the simply supported embedded steel beam under the UDL

1) Geometrical characteristics

The second-moment of area and the sectional modulus of the steel beam could be calculated as

$$I = \frac{bh^3}{12} - \frac{2b'h'^3}{12} = \frac{100\times150^3}{12} - \frac{2\times47\times134^3}{12} = 9277185.33\ \text{mm}^4$$

$$W = \frac{I}{h/2} = \frac{9277185.33}{(150/2)} = 123695.80\ \text{mm}^3$$

where b is the flange width of the steel beam, h is the overall depth of the steel beam, b' is the net flange width on one side and $b' = (100 - 6)/2 = 47$ mm, and h' is the depth of the web and $h' = 150 - 2\times8 = 134$ mm.

2) Reduced material characteristics

Under the action of the external fire, the maximum temperature in the embedded steel appeared in the lower flange at the mid-span, which coincided with the point with the maximum bending moment and deflection of the steel beam under the static loading at room temperature. Therefore, the calculation of the load bearing capacity of a steel beam under fire would mainly be focused on the calculation of the maximum bending moment and deflection at the mid-span. The temperature at the mid-span of the steel beam reached 416°C after a two-hour standard fire. According to BS EN 1993-1-2 [17], both the elastic modulus and yield strength of steel would drop at this temperature. As can be seen from Figure 10, the reduction coefficients could be taken as 0.685 and 0.97 for both properties, respectively, i.e.

$$E = 0.685 \times 210000 = 143850\ \text{N/mm}^2$$
$$f_y = 0.97 \times 400 = 388\ \text{N/mm}^2$$

3) Maximum bending moment

According to BS EN 1993-1-1 [30], the bending moment capacity could be related to the assumed maximum UDL w as

$$M_{c,Rd} = \frac{W_{pl}\ f_y}{\gamma_{M0}} = \frac{123695.80\times388\times10^{-6}}{1.0} = M_{Ed} = \frac{wL^2}{8} = \frac{w\times1.0^2}{8} = \frac{w}{8}$$

i.e. $M_{c,Rd} = 47.994$ kNm and $w = 383.952$ kN/m

4) Deflection

According to BS EN 1993-1-1 [30], the estimated mid-span deflection under the UDL $w = 383.952$ kN/m, δ_{max}, would be:

$$\delta_{max} = \frac{5wL^4}{384EI} = \frac{5\times 383.952\times 1000^4}{384\times 143850\times 9277185.33} = 3.746 \text{ mm}$$

$$\delta_{limit} = \frac{L}{360} = \frac{1000}{360} = 2.778 \text{ mm} < \delta_{max} = 3.746 \text{ mm}$$

The steel beam failed due to the exceeded deflection under the UDL w = 383.952 kN/m. Thus, letting the maximum deflection at the mid-span be equal to its limit would yield the maximum UDL the steel beam could support as follows

$$\delta_{max} = \delta_{limit} \quad \text{or} \quad \frac{5\times w\times 1000^4}{384\times 143850\times 9277185.33} = \frac{1000}{360}$$

i.e. w = 284.698 N/mm = 284.698 kN/m

At this time, although the bearing capacity could reach up to 383.952 kN/m, the deflection would exceed its limit. Therefore, if the deflection requirements were met, the final bearing capacity would still need to be further reduced. However, in practice, since the outer Glulam beam was not completely burned out, it served as a T-shape coating outside the steel beam to limit its excessive deflection and the buckling failure of its upper flange and web. Thus, the ultimate bearing capacity would still be governed by the bending moment capacity.

5. Comparative analyses

5.1 Steel beam

A steel beam model with the same size as the embedded steel section in the standard CST beam was created in ABAQUS (without bolt holes), with the same step, amplitudes and interactions assigned as well. The calculation results for t = 15 min were selected and are shown in Figure 14 below.

It can be seen from the figure that, without the protection of the outer Glulam, the temperature of the steel beam rapidly reached above 600°C within only 15 min, and the highest temperature in the web was nearly 700°C. The steel beam exhibited "thermoplastic" phenomenon, and most of the strength was lost. At this moment, even a small load was applied on the steel beam, its web would quickly buckle due to insufficient strength and stiffness, leading to the failure of the steel beam. By looking at the temperature field distribution of the standard CST beam at t = 15 min (see Figure 11(a)), the temperatures in the steel beam did not rise remarkably and its bending performance should be not significantly different from the static calculation results at room temperature.

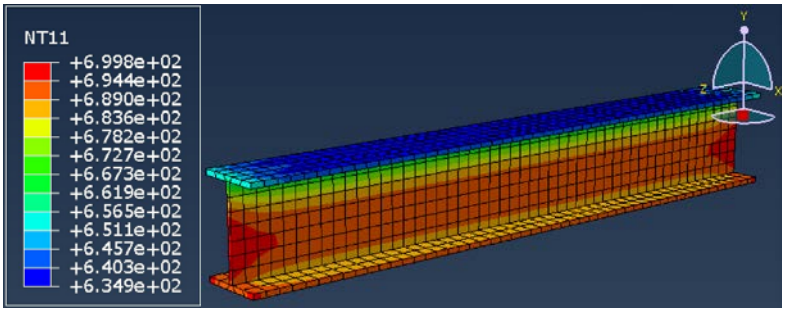

Figure 14. Node temperature contour of the pure steel beam at t = 15 min

5.2 Glulam beam

The Glulam beam model (without embedded steel and through bolts) was created in ABAQUS with the same size as the external Glulam beam for the standard CST beam. The calculation results at t = 15 min and 60 min were selected and are shown in Figure 15.

It is apparent that the overall temperature field distributions and charring depth of the Glulam beam, which was about 16.7 mm, were similar to those of the CST beam. This means that the steel bolts, which brought the heat from the outside fire environment, did not have a critical effect on the overall temperature distributions of the Glulam beam during the first heating hour. As for its bending capacity, it could be estimated by using the reduced cross-section method, described in BS EN 1995-1-2 [21]. In this case, the effective cross-section dimensions of the Glulam beam were smaller than 160 mm × 230 mm under external loads. However, with the introduction of the steel beam, the overall bearing capacity can be a sum of the respective capacities of both Glulam and steel beams [14], which was greatly improved. Moreover, with the increase of the fire exposure time to one hour, the

external Glulam gradually lost most of its strength, with the charring depth to 45.2 mm, while the steel beam material strength reduction was relatively small. Thus, the overall combined value would still have a good bearing capacity or resistance to the external loads.

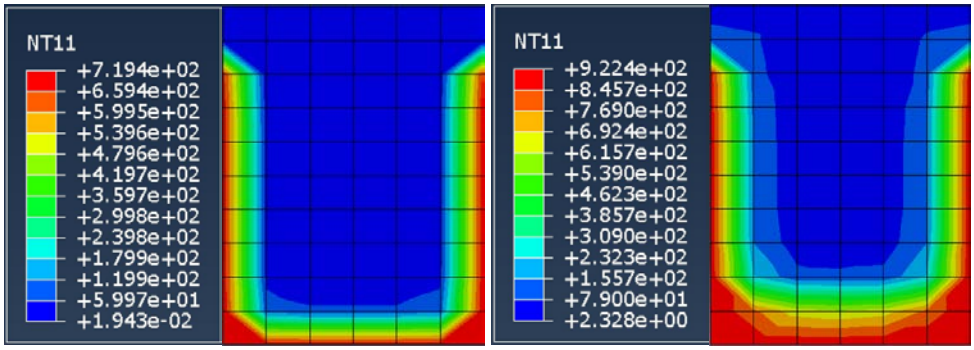

Figure 15. Temperature distribution contours of the pure Glulam beam section at t =15 min and 60 min

6. Parametric Study

In order to improve the simulation efficiency in ABAQUS, the model was established as a quarter of the entire beam (see Figure 16), and the cut quarter cross-section could be defined to explain its symmetry by creating new boundary conditions.

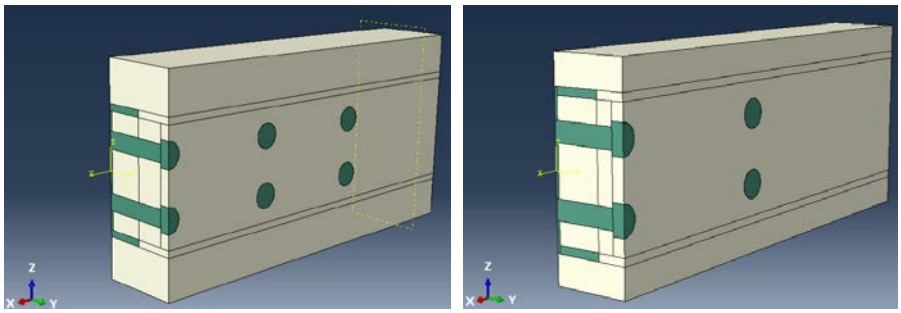

(a) Model with reduced bolts spacing **(b)** Model with reduced Glulam protection thickness

Figure 16. Adjusted CST beam models in ABAQUS

6.1 The adjusted CST beam model with the reduced bolt spacing

6.1.1 Charring characteristics

The charring depth was basically the same as that of the standard beam without significant difference for up to one-hour fire exposure (see Figure 17). However, when the fire action extended to 2 hours, the node temperatures of the bottom of the Glulam beam had reached 400°C, and thus it was considered that all the protection layers of Glulam failed.

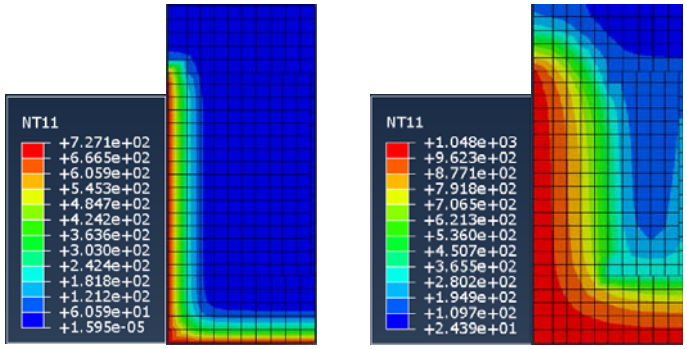

(a) t = 15 min **(d)** t = 120 min

Figure 17. Node temperature contours of the Glulam section of an adjusted CST beam with the reduced bolt spacing at t = 15 min and 120 min

6.1.2 Temperature field of the embedded steel beam

By comparing Figures 8 and 18, it can be found that in terms of the overall distributions of the temperature field, due to the decrease in the bolt spacing, more heat from the external fire field penetrated into the internal steel beam through the bolts, specifically the bolt hole areas in the web, which resulted in the heat conduction to the surrounding area and eventually the overall steel temperatures. For instance, for t = 60 min, the average temperature of the web had exceeded 130°C, while the average temperature of the standard beam was only 110°C. In addition, the smaller bolt spacing made it easier to connect and superimpose the temperature fields around adjacent bolt holes. This could be verified by the fact that the temperature field near the areas of the bolt holes of the standard beam for t = 15 min only had a tendency, while the current beam model had completed most of the temperature field connections. Consequently, due to this strengthened superimposition impact, after burning in the fire field for 120 min, the lower flange of the embedded steel beam had reached 462°C. Compared with that of the standard CST beam, namely 416°C, the temperature rose significantly.

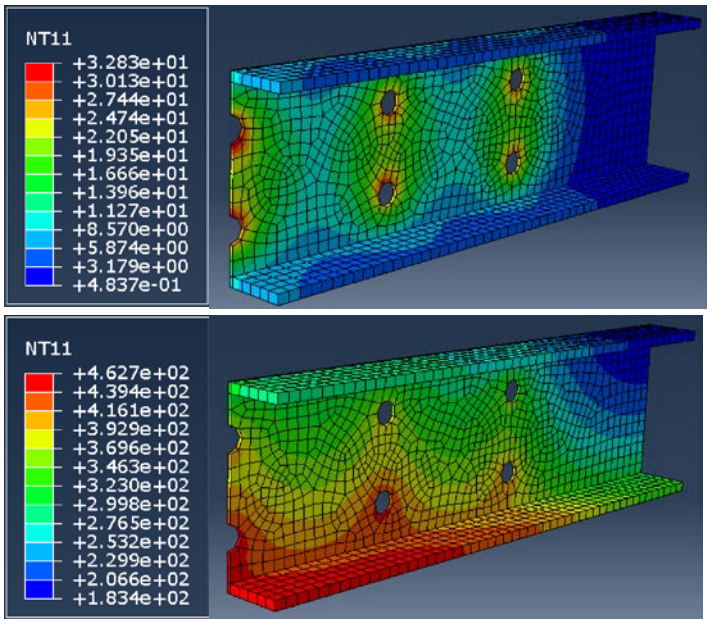

(a) t = 15 min

(b) t = 120 min

Figure 18. Temperature contours of the half steel beam with the reduced bolt spacing at t = 15 min and 120 min

6.1.3 Estimation of the consequent displacement field

The reduction in the bolt spacing and the increase in the number of bolts per unit length could improve the composition robustness of the Glulam and steel beams, and additionally better the bending performances under room temperature. For structural fire design and analysis, however, this adjustment would pump more external heat into the internal steel beam, making the temperatures in its web rise faster. Especially after the structure was exposed to fire for 2 hours, the Glulam at this moment was completely burnt out, and the lower flange of the embedded steel beam would be exposed to the fire. If a continuous fire field was applied, the steel beam would be heated up quickly and largely lose its strength. In other words, this would finally weaken the protection ability of Glulam, and the steel beam would lose its bearing capacity faster than the standard CST beam.

6.2 The adjusted CST beam model with the reduced Glulam protection thickness

6.2.1 Charring characteristics

By comparing Figures 11 and 19, it can be found that there was a big difference between the charring depth of the adjusted model at t = 1 hour (29.6 mm) and that of the standard CST beam (44.1 mm), but there was no much difference between the corresponding charring depths of 15.2 mm and 15.8 mm at t = 15 min. This could be because when the protection layer thickness of the Glulam decreased with the increase of the fire duration, the protection layer was burned off, heat gradually came in to contact with the bottom flange of the steel beam, and thus the steel beam could well transfer the heat evenly to other areas of the beam for a better thermal conductivity. This would help absorb some heat from the Glulam. When the action time was small, the protection effect of the Glulam still played a leading role, and thus the charring depth difference was not so big.

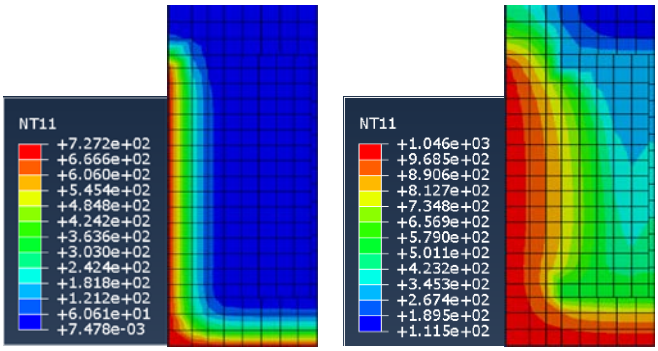

(**a**) t = 15 min (**b**) t = 120 min

Figure 19. Node temperature contours of the Glulam section of an adjusted CST beam with the reduced Glulam protection layer at t = 15 min and 120 min

6.2.2 Temperature field distributions of the embedded steel beam

By comparing Figures 8 and 20, it can be found that because of the reduced protection layer thickness of the Glulam, heat from the fire environment would be able to more quickly penetrate into the bottom flange of the embedded steel beam, and this led to the quicker rises of the overall temperatures in the steel beam. In particular, at t = 60 min, the average temperature of the lower flange had exceeded 230°C, while the average temperature of the standard beam was only 120°C. This huge difference became more obvious in the 120-min temperature field. At this moment, the maximum node temperature occurred at the mid-span of the lower flange and reached almost 670°C, which was much higher than that of the standard CST beam model, namely 416°C, and would cause excessive reductions in the material properties. Hence, reducing the thickness of the Glulam protection layer would greatly increase the heating rate of the embedded steel beam.

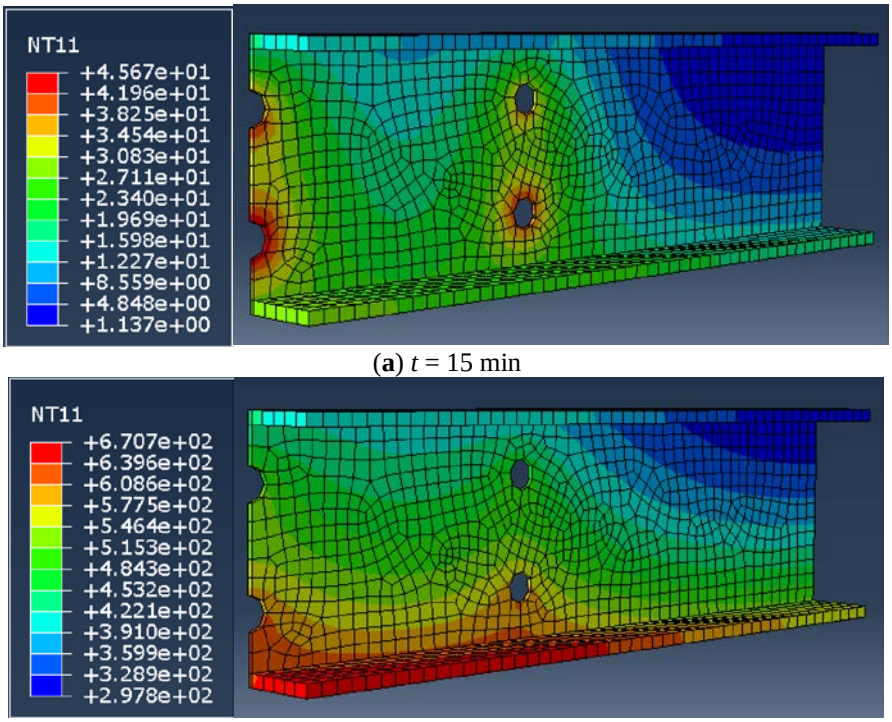

(**a**) t = 15 min

(**b**) t = 120 min

Figure 20. Node temperature contours of the half steel beam with the reduced Glulam protection thickness at t = 15 min and 120 min

7. Conclusions

In this research, based on the finite element analysis software ABAQUS, numerical simulations and analyses of the temperature field and displacement field of the standard CST beam were conducted in a sequential coupling way. Through the analysis on the temperature field results, the validity of the calculation model was verified, and

the heat transfer process and distribution characteristics of this type of CST beam under fire conditions were summarised. By analysing the results of the displacement field, the flexural performances of the embedded steel beam after the fire were determined. Additionally, the corresponding steel beam and Glulam beam models were simulated for comparison, and the advantages of this type of CST beam in the structural fire design were verified. Finally, by adjusting the parameters of the standard CST beam model, the effects of reducing the bolt spacing and the Glulam protection layer thickness on the temperature fields of the CST beam were analysed, respectively. The following conclusions on the research results can be drawn.

1) For the standard CST beams:

a) Consistent to previous researchers' findings, the simulated charring depth of the Glulam increased but the charring rate decreased gradually during the 2-hour standard fire.

b) The temperature rises in the whole structure started from the outer Glulam and steel bolts. The carbonisation of the Glulam timber would block further heat transfer, but the heat from the external fire field would still enter the inner CST beam through the exposed steel bolts, causing the local heating of the embedded steel beam and eventually the overall temperature rises in the steel beam.

c) After the 120-min standard fire, the 50 mm external Glulam protection layer was almost completely burned out and charred. However, this could effectively protect the embedded steel beam, except the areas of the bolt holes at the mid-span, from experiencing excessive temperature increases and help maintain most of its mechanical properties and structural performances.

d) Under the uniformly distributed load, the embedded steel beam showed fairly good flexural resistances, and the stress and displacement distributions were not largely different from those at normal temperature.

2) For the individual steel beam and Glulam beam:

a) Without the protection of Glulam, the individual steel beam, after the 15-minute standard fire, quickly lost most strength due to thermoplastic phenomenon. Meanwhile, the charring depth and rate of the individual Glulam beam, after the 60-minute standard fire, presented no large differences from those of the standard CST beam.

b) By comparison, the protection effects provided by Glulam and its contributions in maintaining the load bearing capacity of a structural beam for a long time in the fire field were further verified.

3) For two types of the adjusted CST beams:

a) Although reducing the bolt spacing, i.e. increasing the number of bolts per unit length, could improve the composition integrity of the two materials, but under fire conditions, this reversely promoted the temperature field superposition of the bolt hole areas in the steel beam web and accelerated the heating rate of the embedded steel beam, and thus the ultimate load bearing capacity and refractory limit could be reduced.

b) Although reducing the thickness of the Glulam protection layer, i.e. reducing the self-weight of the CST beam and improving the structural and economic efficiencies, the temperature field distributions of the composite structure were largely affected. After the 60-minute standard fire, the Glulam protection layer was completely burned out, and the continuous heating would lead to a rapid rise in the temperature in the embedded steel beam, and finally the overall failure of the composite steel-timber beam structure would happen.

In general, the structural fire analysis on the new type of CST beam, carried out through the numerical simulations in this study, was relatively abundant, after verifying its potential advantages in fire engineering, evaluating its flexural performances under the two-hour standard fire and discussing the impacts of the variations in the bolt spacing and Glulam protection thickness on the structural fire performances of the CST beam. In the future, the comparative explorations between the laboratory combustion data and numerical simulation results as well as the parameter optimisation analyses based on the secondary development of finite element software will be the focus of subsequent researches.

Acknowledgements

This project is supported by both the School of Computing, Engineering and Built Environment at Glasgow Caledonian University, Scotland, UK, and Department of Civil Engineering, School of Architectural Engineering, Jinling Institute of Technology, Jiangsu Province, China.

Funding

This project was supported by The Natural Science Fund for Colleges and Universities in Jiangsu Province (Grant No. 17KJB560004), The Jinling Institute of Technology High-level Personnel Work Activation Fee to Fund Projects (Grant No. jit-b-201608), and The Program of National Natural Science Foundation (Grant No. 51608103).

8. References

[1] Liu Z, Jia H, Wu C, Li M, Chen X. Research on the life cycle management method of 3D visualized fabricated steel structure based on BIM technology. In: Proceedings of Jiangsu Steel Structure Conference, Nanjing, China, 238-242, October 2019.

[2] Zhang Y, Zhou X. Design Principle of Steel Structure (2nd Ed), Higher Education Press, Beijing, China, 2004.

[3] Bai R, Jiang Z. Research on steel-timber composite structure. Journal of Hebei Institute of Architecture and Civil Engineering. 2016;34(3):75-78.

[4] Pan F. Experimental Research and Finite Element Analysis on Steel-Timber Combined Members. Master's Thesis, Southeast University, Nanjing, China, 2008.

[5] Fujita M, Sakai J, Oda H, Iwata M. Building system for a composite steel-timber structure. Steel Construction. 2014;7(3):183-187. DOI: 10.1002/stco.201410032.

[6] Wang X, Chen Z, Bai J, Li S, An Q. Research status and development prospect of timber-steel composite structure. In: Proceedings of National Steel Structure Academic Annual Conference, Kunming, China, April 2011.

[7] Product Guide: Glulam. Available online: https://www.apawood.org/publication-search?q=X440&tid=1 (Accessed on 10 November 2020).

[8] Japan Association of Building Construction Technicians (JABCT). 100 Selected Typical Examples of Structural Technology in Japan. China Building Industry Press, Beijing, China, 2005.

[9] Fujita M, Iwata M. Bending test of the composite steel-timber beam. Applied Mechanics and Materials. 2013;351-352:415-421.

[10] Luo J, Li Q, Deng R. Numerical analysis on flexural performance of a new kind timber-steel composite beams. Low Temperature Architecture Technology. 2017;39:46-48.

[11] Chiniforush AA, Valipour H, Akbarnezhad A, Bradford M. Steel-timber composite (STC) beams: Numerical simulation of long-term behaviour. Eurosteel. 2017;1(2-3):2051-2059.

[12] Wang J, Duan S. Experimental analysis of eccentric pressure behaviour of steel-timber composite columns. Building Technology. 2019;46(9):16-17.

[13] Hua Q, Gao Y, Meng X, Diao Y. Axial compression of steel-timber composite column consisting of H-shaped steel and Glulam. Engineering Structures. 2020;216:1-12.

[14] Le T, Tsai M. Behaviour of timber-steel composite with dowel connection under fire. Key Engineering Materials. 2019;803:195-199.

[15] Liu Y, Chen Z, An Q, Chen B. Experimental investigation on lateral resistance performance of light timber-steel hybrid shear wall. Journal of Tianjin University (Science and Technology). 2017;50:78-83.

[16] Zhou X, Li Z, Wang R, Shi Y. Study on load-carrying capacity of the cold- formed steel joists-OSB composite floor. China Civil Engineering Journal. 2013;46(9):1-11.

[17] Keipour N, Valipour HR, Bradford MA. Steel-timber composite beam-to-column joints: Effect of connections between timber slabs. Journal of Constructional Steel Research. 2018;151:132-145.

[18] Hassanieh A, Valipour HR, Bradford MA, Sandhaas C. Modelling of steel-timber composite connections: Validation of finite element model and parametric study. Engineering Structures. 2017;138:35-49.

[19] Knobloch M. Structural fire design - developments in research and assessment of fire in steel and composite structures. Eurosteel. 2017;1(2-3):133-142.

[20] BSI. BS EN 1993-1-2:2005 Eurocode 3 Design of Steel Structures - Part 1-2 General Rules - Structural Fire Design. British Standards Institution (BSI), London, UK, 2005.

[21] BSI. BS EN 1995-1-2:2004 Eurocode 5 Design of Timber Structures - Part 1- 2 General - Structural Fire Design. British Standards Institution (BSI), London, UK, 2004.

[22] Zhang J, Liu Z, Xu Y, Ma S, Xu Q. Experimental and numerical study on the charring rate of timber beams exposed to three-side fire. Science China-Technological Sciences. 2012;55(12):3434–3444. DOI: 10.1007/s11431-012-4996-1.

[23] 3D EXPERIENCE, ABAQUS; Version 2020 [Computer software]; Dassault Systèmes Simulia Corp., Providence, RI, USA. 2019.

[24] ABAQUS 6.14: Analysis User's Guide. Available online: https://www.academia.edu/28334906/Abaqus_Analysis_Users_Guide/ (accessed on 20 May 2021).

[25] Zhu Y, Cai W. Introduction to ABAQUS/Standard Finite Element Software - ABAQUS/CAE Edition. Tsinghua University Press, Beijing, China, 2003.

[26] Zhang Y. Experimental Study on the Fire Performance of Post-and-Beam Timber Structure with Bolted Steel-Timber Connection. Master's Thesis, Southeast University, Nanjing, China, 2016.

[27] Ohene AA. Modelling the Fire Performance of Hybrid Steel-Timber Connections. Master's Thesis, Carleton University, Ottawa, Canada, 2014.

[28] ISO. ISO 834-1 Fire Resistance Tests - Elements of Buildings Construction - Part-1 General Requirement, International Organization for Standardization (ISO), Switzerland, 1999.
[29] Li G, Wang W. State-of-the-art and development trend of fire safety research on steel structures. China Civil Engineering Journal. 2017;50(12):1-8.
[30] BSI. BS EN 1993-1-1:2005 + A1:2014 Eurocode 3 Design of Steel Structures – Part 1-1 General Rules and Rules for Buildings. The British Standards Institution (BSI), London, UK, 2005.